Master's Thesis

Design of High Performance Silicon Anode for Li-ion batteries

Wooyeong Choi

Department of Energy Engineering
(Battery Science and Technology)

Graduate School of UNIST

2019

Design of High Performance Silicon Anode for Li-ion batteries

Wooyeong Choi

Department of Energy Engineering
(Battery Science and Technology)

Graduate School of UNIST

Design of High Performance Silicon Anode for Li-ion batteries

A thesis
submitted to the Graduate School of UNIST
in partial fulfillment of the
requirements for the degree of
Master of Science

Wooyeong Choi

11.30
. 2018
Approved by

_____

Advisor
Nam-Soon Choi

Design of High Performance Silicon Anode for Li-ion batteries

Wooyeong Choi

This certifies that the thesis of Wooyeong Choi is approved.

11. 30. 2018

Signature

_____

Thesis supervisor: Nam-Soon Choi

Signature

_____

Soojin Park

Signature

_____

Seok Ju Kang

Contents

List of Figures

Abstract

Today, Li-ion batteries (LIB) have been used in many areas such as mobile electronics, electric vehicles, and large-scale smart grids. Since the first commercialized Li-ion batteries developed by SONY in 1991, LIBs have made a lot of advances and successfully used in many areas. However, with the advent of electric vehicles, energy storage system, and smart grid, high energy and power density required for LIB have increased rapidly. To meet the increasing demand for high-quality LIBs, various researches are doing such like safety, cyclability, charge rate, gravimetric and volumetric energy density. In addition, we try to develop next-generation LIB to improved performances dramatically.

Herein, we demonstrate the LIBs and next-generation LIB anode materials.

In chapter 1, we introduce basic decription of Li-ion battery system(LIBs), anode materials for LIBs, and challeges in silicon anode.

In chapter 2, we introduce a scalable method of selective extraction of high-quality nano-silicon from industrial slag. The extraction process is based on thermochemical reduction of silica. Herein, we use a mixture of metal (e.g. aluminum) and metal halide (e.g. aluminum chloride), we can extract nano-silicon from at low temperature. Owing to our silicon source industrial slag, synthesized nano-silicon is very cost-effectiveness. Interestingly, extracted nano-silicon have high purity, regular size (200~300nm), and regular structure, thus it shows improved cyclability.

In chapter 3, we introduce a facile method of synthesis of unique structure Si/C composite. Herein, we use a Si/SiC wafer waste, silicon chip as the silicon source. SiC can be oxidized endlessly. Owing to SiC property, we can control the oxidation contents of silicon chip. And using polyacrylonitrile polymer and oxidized silicon chips, we synthesize unique structure Si/C composite. Owing to unique structure of Si/C composite, it shows improved cyclability.

Chapter 1. Introduction of Li-ion batteries

1.1. Introduction

1.1.1. Basic decription of Li-ion batteries

Nowadays, the reckless use of fossil fuels creates problems such as depletion of fossil fuels and the generation of the CO_2 gases[1-3]. Emission of CO_2 gases creates not only global warming but also acidifies the ocean[1-3]. To solve these problems, the interest in renewable energy is growing and especially Li-ion batteries (LIBs) are starting to receive much attention as an energy storage device[1-2,4]. In the 1990s, SONY has firstly commercialized the LIBs[5-6]. The LIBs are composed of lithium cobalt oxide cathode (LCO), polymer separator, an organic electrolyte, and carbonaceous anode[7]. Now they have been used in various areas such as energy storage system (ESS), electric vehicles, mobile electronics, and large-scale smart grids[7].

LCO is very attractive cathode materials and mainly used in conventional LIBs, because it has several advantages such as high theoretical capacity (274 mAh/g), high discharge voltage, and good cycling performance[11-13]. However, LCO has some limitations such as high cost, low thermal stability, and irreversible structural change during deep cycling[14].

On the other hand, graphite is commercially available anode materials, because it has several advantages such as low cost, high electrical conductivity, high Li^+ diffusivity, and low anodic potential[15-17]. However, graphite has some limitations such as small theoretical capacity (372 mAh/g) and Li^+ intercalation at the basal plane in graphite[18-20].

Organic electrolyte is mainly used by combining linear carbonate with cyclic carbonate, and it shows high ionic conductivity and electrochemical stability[21]. As another key component, polyethylene and polypropylene are mainly used as LIB separator which can physically separate cathode and anode and provide the pathway of Li-ions and electrolytes[22].

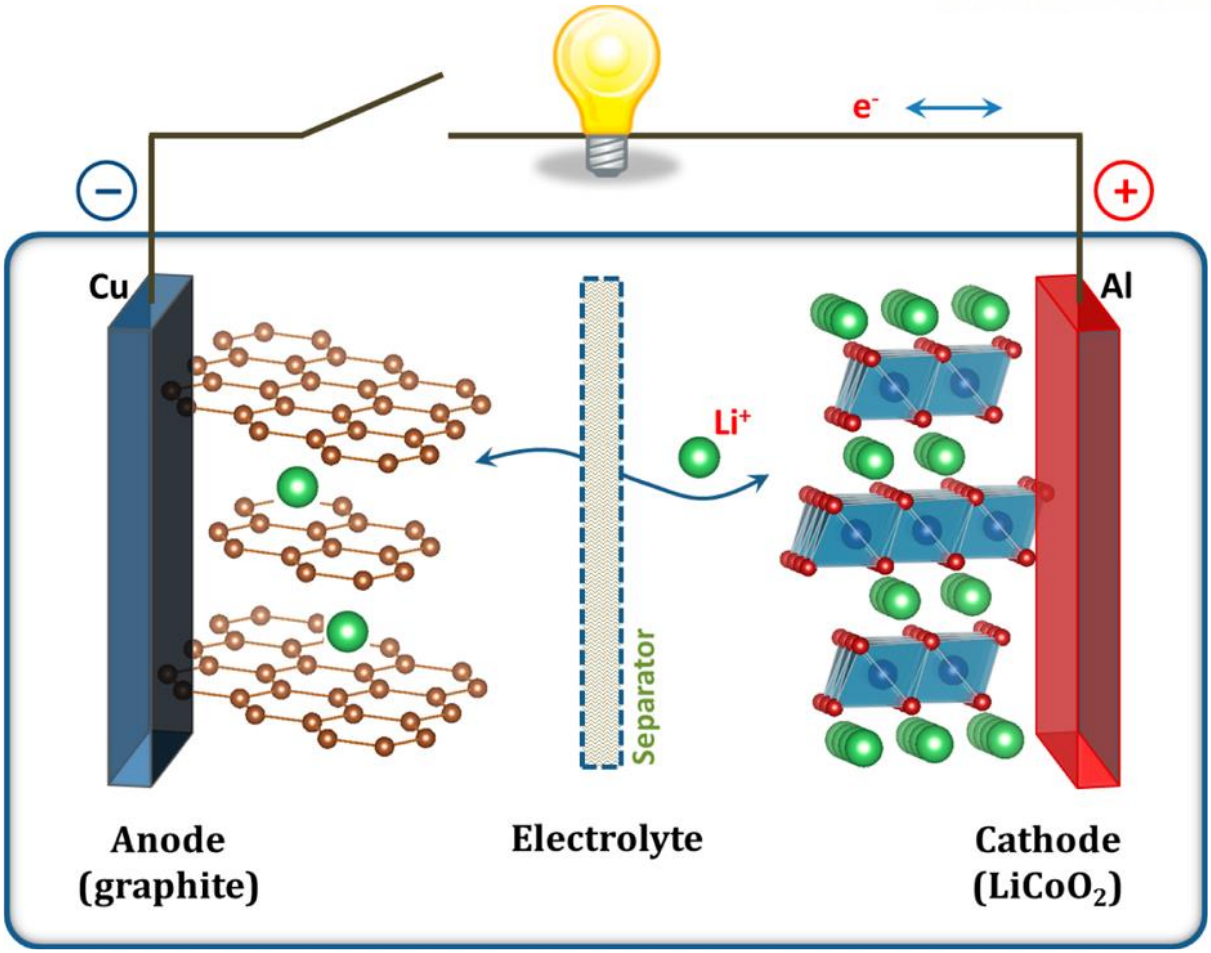

Figure 1.1. Schematic illustration of commercialized Li-ion batteries[2].

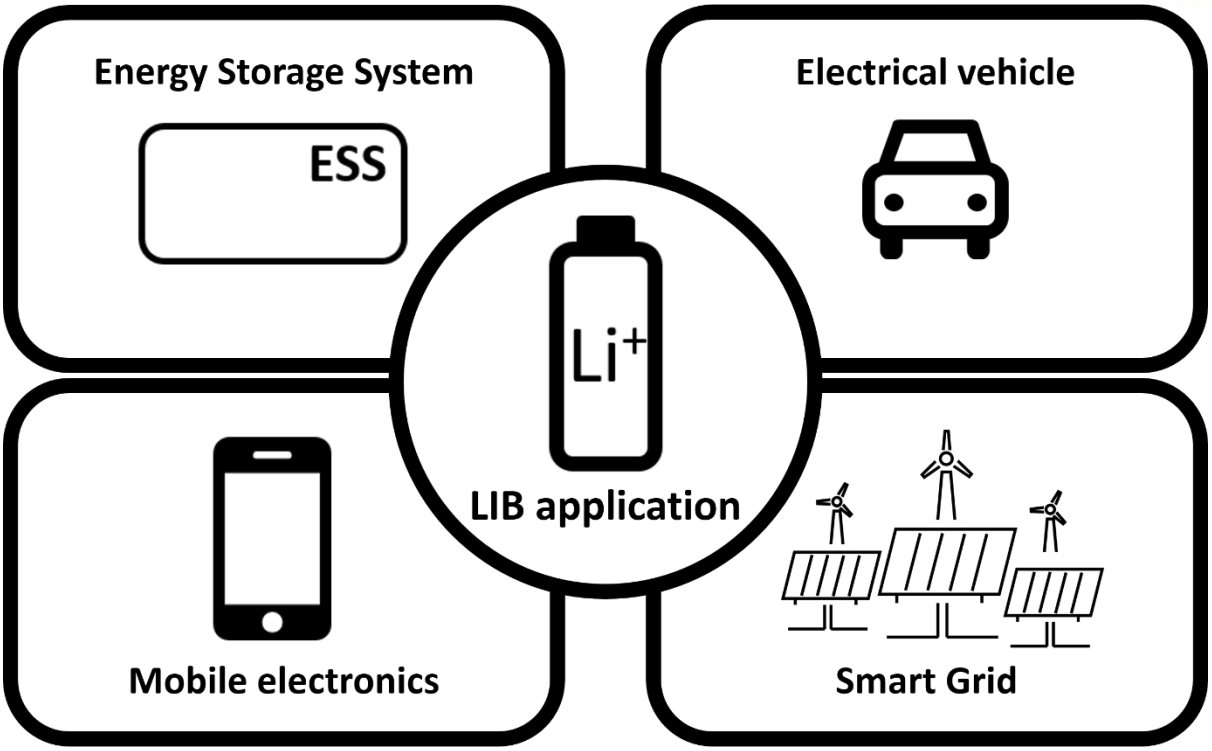

Figure 1.2. Various applications of Li-ion batteries.

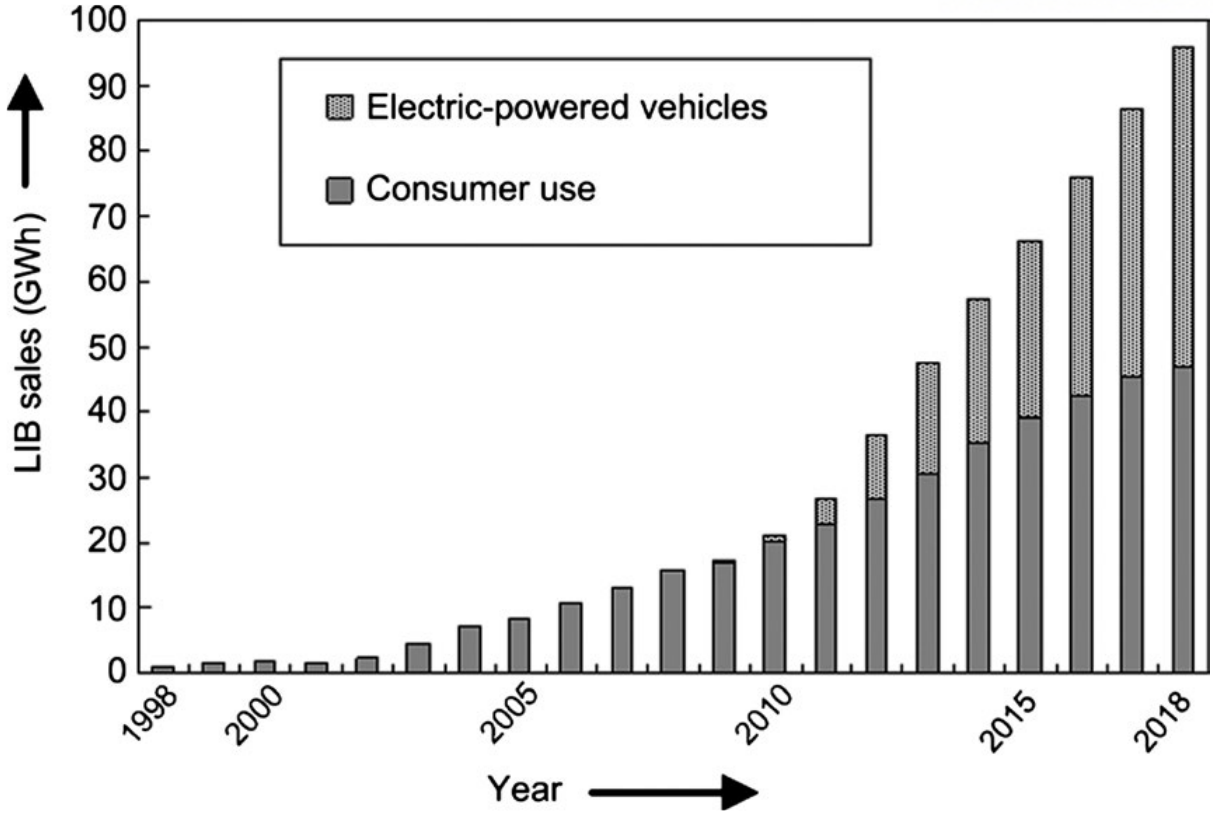

Figure 1.3. Growth of Li-ion batteries market[23].

1.1.2. Anode materials choice for Li-ion batteries

LIB anode materials can be classified into three main categories in terms of reaction mechanism; (i) (de)intercalation (ii) (de)alloying, and (iii) conversion[7,24].

Carbonaceous materials are representative materials with (de)intercalation mechanism and have a layered structure[7,17,24]. Owing to the layered structure, lithium ion can easily move in and out of its lattice space reversibly[15-17]. Owing to its structural stability, (de)intercalation materials show excellent cyclability in Li-ion batteries[15-17]. However, carbonaceous anode materials have a fatal drawback such as low theoretical capacity (372 mAh/g)[18-20]. This drawback hinders its applications in high energy and power density Li-ion batteries.

Conversion reaction commonly works on transition metal oxide compound[25-26]. This conversion reaction proceeds to full reduction of transition metal to its metallic state, so that it shows remarkable high capacity[25]. Many transition metal compounds have no empty space in their structure. As a result, in transition metal, there is no insertion reaction and only conversion reaction can occur and show high capacity[7]. However, conversion anode materials have a fatal drawback such as large voltage hysteresis that causes poor energy efficiency[25-26]. This is the biggest drawback for practical application for Li-ion batteries.

Tin and silicon are representative materials for (de)alloy anode materials for Li-ion batteries[27-28]. These (de)alloy materials have several advantages such as high abundance, low price, and high theoretical capacity[29-31]. Owing to aforementioned reasons, many researches are focusing on (de)alloy materials as anode materials for Li-ion batteries[29-31]. However, (de)alloy materials have a fatal drawback such as dramatic volume change during the (de)alloying process[32]. It causes the loss of contact between composite electrode and current collector, leading to very poor cycling performance[32]. This drawback prevents the commercialization of (de)alloy materials as anode materials for Li-ion batteries.

In addition, nowadays, there have been a lot of researches on various materials such as organic materials and Li-metal as anode materials for Li-ion batteries[33-35].

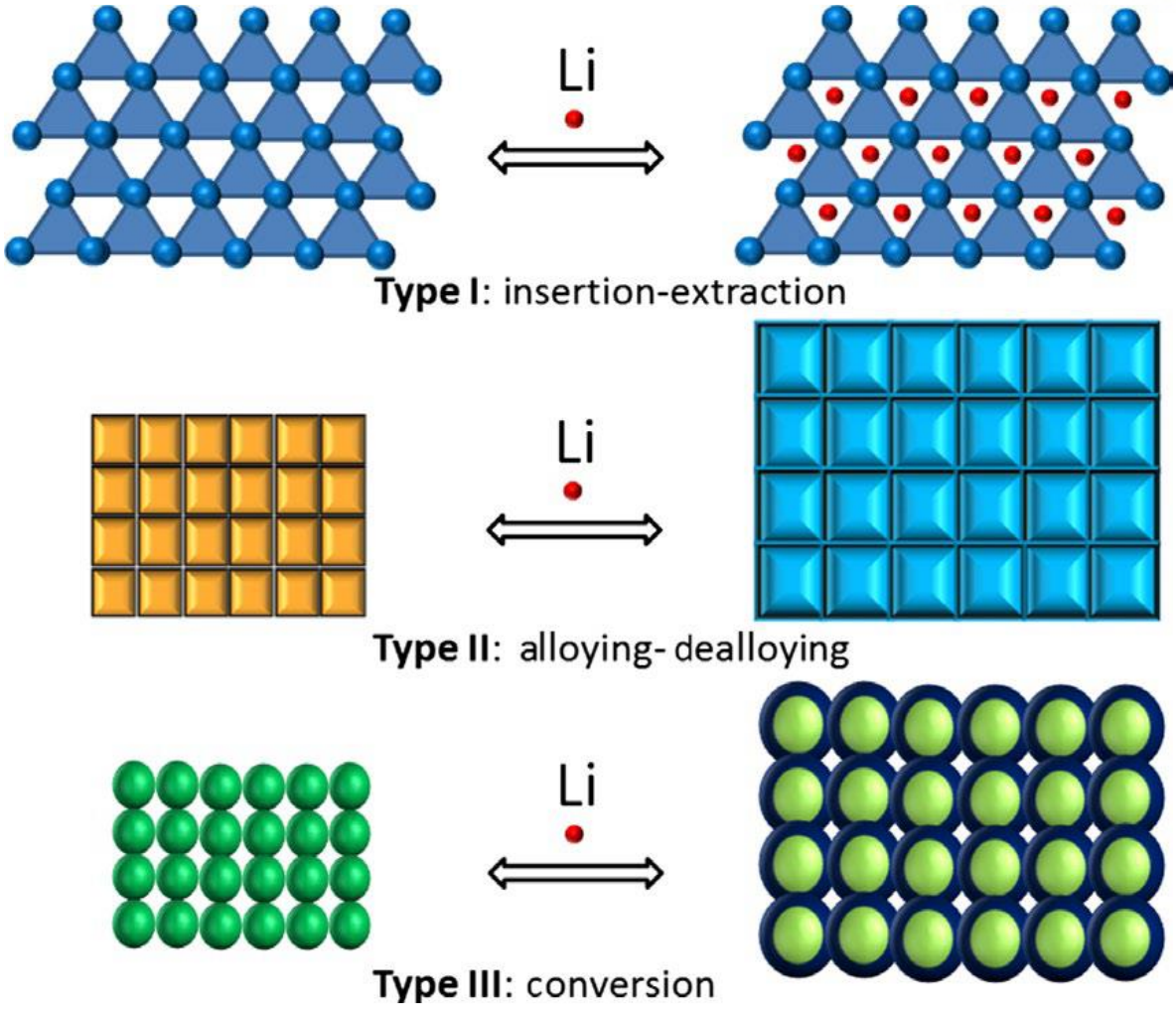

Figure 1.4. Schematic illustration of different mechanisms of reversible lithium ion storage in anode materials[24].

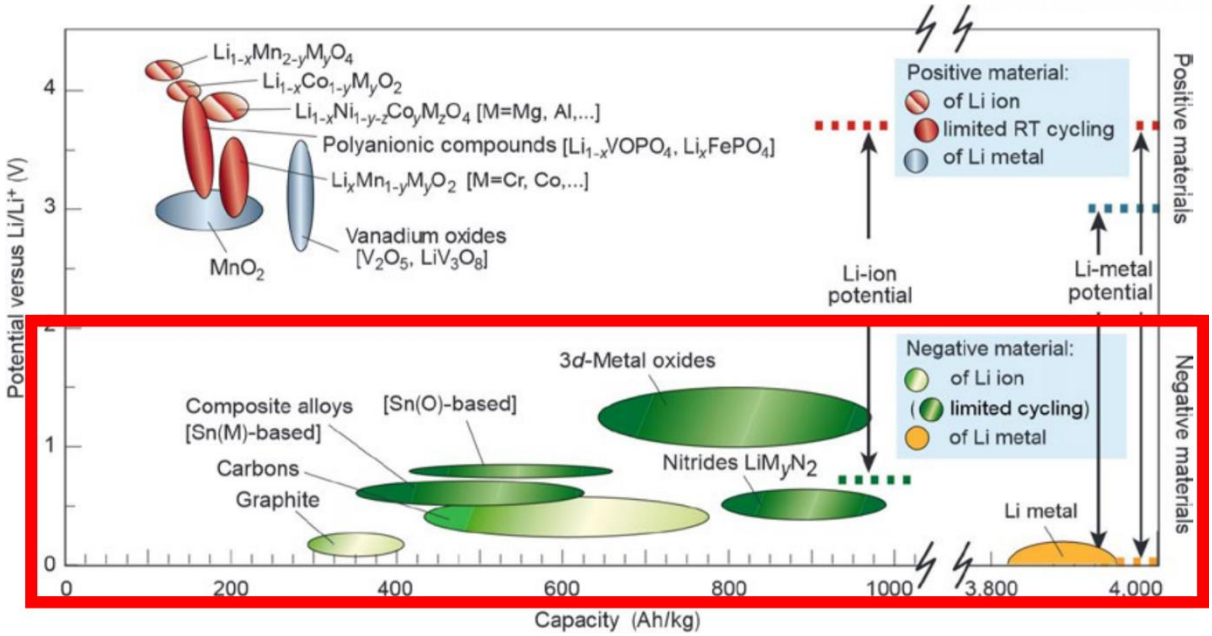

Figure 1.5. Voltage versus capacity for positive- and negative- electrode materials[4].

1.1.3. Challenges in silicon anode

After Li-ion battery (LIB) was commercialized by SONY in 1991, it began to be used in all aspect of society[5-6]. Battery market has been increasing rapidly[23]. However, current practical LIBs are hard to meet the demand for increasing energy and power density[4-5]. To solve this problem, many various researches have been doing today.

Silicon is considered as one of the most promising anode materials for the next-generation LIBs, because silicon has many advantages: First, it has the highest theoretical capacity (4200 mAh/g) that is more than 10 times higher than commercialized graphite anode[36-37]. Second, it has relatively low anodic potential (below 0.4V vs. Li/Li^+)[36-38]. Third, it is the third abundant element in the earth[29-30]. Lastly, it is eco-friendly source[29-30].

However, silicon unfortunately has fatal drawback which has dramatic volume change during charge/discharge process[29-30,32]. Also, silicon semiconductor has intrinsically low electrical conductivity. Further, serious undesirable phenomena occur at the electrode surface such as particle fracture, particle pulverization, electronic contact loss from current collector, and continuous solid-electrolyte-interphase (SEI) layer formation. Due to these issues, silicon anode shows poor cycle performance[39].

To solve these problems, several strategies have been developed including synthesis of nano-sized silicon from cost-effective silicon sources, synthesis of porous silicon, hollow silicon design, and silicon/carbon composite[40].

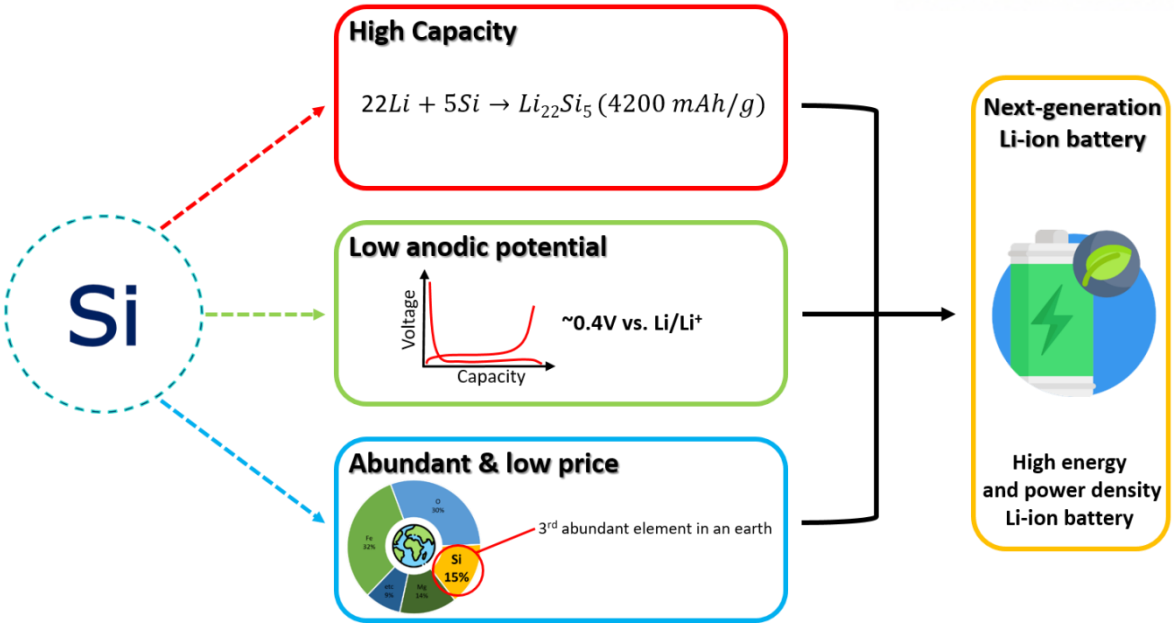

Figure 1.6. Advantages of silicon anode[36].

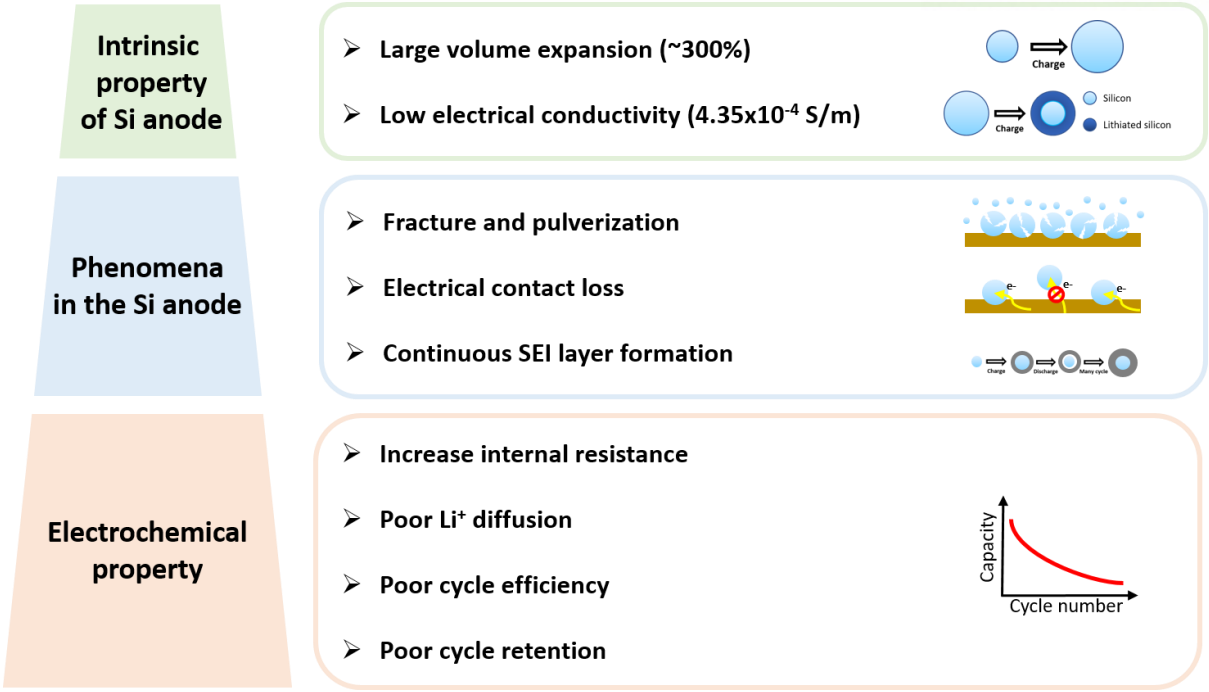

Figure 1.7. Challenges for silicon anode[32].

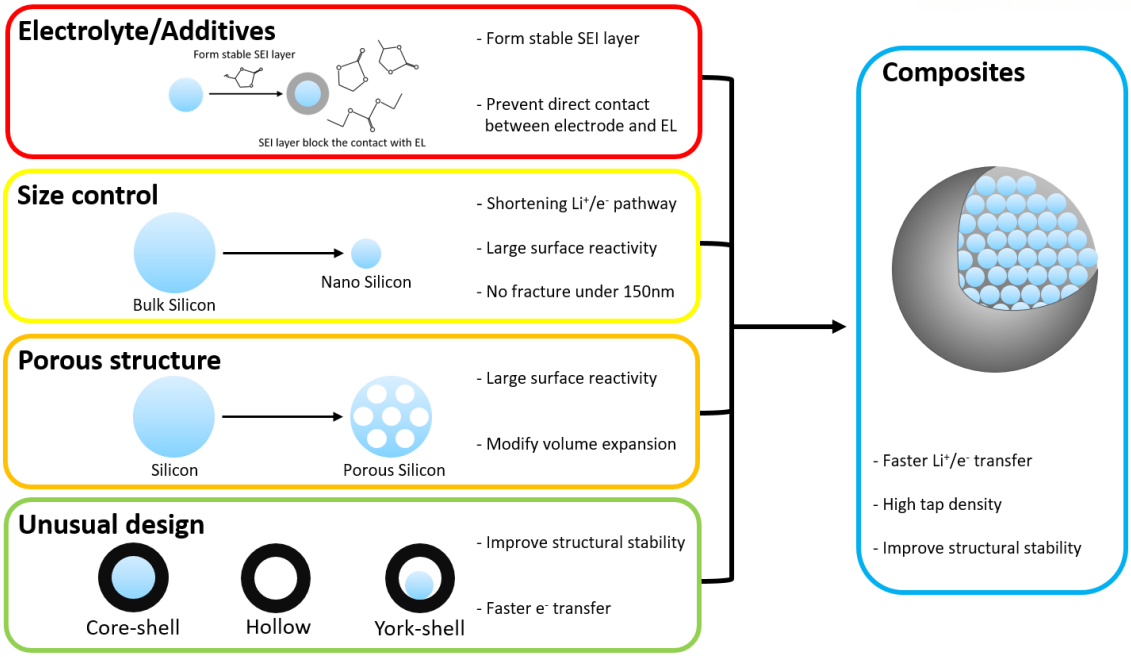

Figure 1.8. Strategies for enhanced performance in silicon anode[41].

1.2 Reference

1. Mikael, H.; Tang, X. Depletion of fossil fuels and anthropogenic climate change-A review. *Power Energy Policy* **2013,** *52*, 797-809.
2. Goodenough, J. B.; Park K. S. The li-ion rechargeable battery: A perspective. *J. Am. Chem. Soc.* **2013,** *135*, 1167-1176.
3. Pacala, S.; Socolow, R. Stabilization Wedges: Solving the Climate Problem for the Next 50 Years with Current Technologies. *Science.* **2004,** 305, 968-972.
4. Tarascon, J.M.; Armand, M. Issues and challenges facing rechargeable lithium batteries. *Nature.* **2001,** 414, 359-367.
5. Scrosati, B.; Garche J. Lithium batteries: Status, prospects and future. *J. Power Sources* **2010,** *195*, 2419-2430.
6. Kodama, T.; Sakaebe H. Present status and future prospect for national project on lithium batteries. *J. Power Sources* **1999,** *81*, 144-149.
7. Palacin, M. R. Recent advances in rechargeable battery materials: A chemist's perspective. *Chem. Soc. Rev.* **2009,** *38*, 2565-2575.
8. Sasaki, T.; Ukyo Y.; Novak P. Memory effect in a lithium-ion battery. *Nat. Mater.* **2013,** *12*, 569-575.
9. Vetter, J.; Novak P.; Wagner M. R.; Veit C.; Moller K. C.; Besenhard J. O.; Winter M.; Wohlfahrt-Mehrens M.; Vogler C.; Hammouche A. Ageing mechanisms in lithium-ion batteries. *J. Power Sources* **2005,** *147*, 269-281.
10. Nitta, N.; Wu, F.; Lee J. T.; Yushin, G. Li-ion battery materials: present and future. *J. mattod.* **2014,** *10*, 040.
11. Pasquier, A. D.; Plitz I.; Menocal. S.; Amatucci. G. A comparative study of Li-ion battery, supercapacitor and nonaqueous asymmetric hybrid devices for automotive applications. *J. Power Sources.* **2003,** 115, 171-178.
12. Goodenough, J. B.; Kim Y. Challenges for rechargeable li batteries. *Chem. Mater.* **2010,** *22*, 587-603.
13. Whittingham, M. S. Lithium batteries and cathode materials. *Chem. Rev.* **2004,** *104*, 4271-4301.
14. Dahn, J. R.; Obrovac, M. Thermal stability of Li_xCoO_2, $LiNiO_2$ and λ–MnO_2 and comsequences for the safety of Li-ion cells. *Solid State Ionics.* **1994,** 69, 265-270
15. Kaskhedikar, N. A.; Maier, J. Lithium Storage in Carbon Nanostructures. *Adv. Mater.* **2009,** 21, 2664-2680.
16. Qi. Y.; Guo. H.; Hector, L. G.; Timmons, Adam. *J. Electrochem. Soc.* **2010,** 157, A558-A566.
17. Peled, E.; Menachem C.; BarTow D.; Melman A. Improved graphite anode for lithium-ion batteries - chemically bonded solid electrolyte interface and nanochannel formation. *J.*

Electrochem. Soc. **1996,** *143*, L4-L7.

18. Bar-Tow, D.; Peled, E.; Burstein. L. A study of Highly Oriented Pyrolytic Graphite as a Model for the Graphite Anode in Li-ion batteries. *J. Electrochem. Soc.* **1999,** 146, 824-832.
19. Tirado, J. L.; Inorganic materials for the negative electrode of lithium-ion matteries: state-of-the-art and future prospects *Mater. Sci. Eng. R: Rep.* **2003,** 40, 103-136.
20. Ji, L. W.; Lin Z.; Alcoutlabi M.; Zhang X. W. Recent developments in nanostructured anode materials for rechargeable lithium-ion batteries. *Energy Environ. Sci.* **2011,** *4*, 2682-2699.
21. Xu, K.; Nonaqueous Liquid Electrolytes for Lithium-Based Rechargeable Batteries. *Chem. Rev.* **2004,** 104, 4303-4418.
22. Zhang, S. S.; A review on the separators of liquid electrolyte Li-ion batteries. *J. Power Sources.* **2007,** 164, 351-364.
23. Yoshino, A.; The Birth of the Lithium-Ion Battery. *Angew. Chem. Int. Ed.* **2012,** 51, 5798-5800.
24. Liu, F.; Song, S.; Xue, D.; Zhang, H. Selective crystallization with preferred lithium-ion storage capability of inorganic materials. *Nanoscale Res. Lett.* **2012,** 7, 149.
25. Poizot, P.; Laruelle, S.; Dupont, L.; Tarascon, J. M. Nano-sized transition-metal oxides as negative-electrode materials for lithium-ion batteries. *Nature.* **2000,** 407, 496-499.
26. Cabana, J.; Monconduit, L.; Larcher, D.; Palacin, M. R. Beyond Intercalation-Based Li-Ion Batteries: The State of the Art and Challenges of Electrode Materials Reactiong Through Conversion Reactions. *Adv. Mater.* **2010,** 22, E170-E192.
27. Thackeray, M. M.; Vaughey, J. T.; Johnson, C. S.; Kropf, A. J.; Benedek, R.; Fransson, L. M. L.; Edstrom. K. Structural considerations of intermetallic electrodes for lithium batteries. *J. Power Sources.* **2003,** 113, 124-130.
28. Larcher, D.; Beattie, S.; Morcrette, M.; Edstrom, K.; Jumas, J. C.; Tarascon, J. M. Recent findings and prospect in the field of pure metals as negative electrodes for Li-ion batteries. *J. Mater. Chem.* **2007,** 17, 3759-3772.
29. Park, C. M.; Kim J. H.; Kim H.; Sohn H. J. Li-alloy based anode materials for li secondary batteries. *Chem. Soc. Rev.* **2010,** *39*, 3115-3141.
30. McDowell, M. T.; Lee S. W.; Nix W. D.; Cui Y. 25th anniversary article: Understanding the lithiation of silicon and other alloying anodes for lithium-ion batteries. *Adv. Mater.* **2013,** *25*, 4966-4984.
31. Nitta, N.; Yushin G. High-capacity anode materials for lithium- ion batteries: Choice of elements and structures for active particles. *Part. Part. Syst. Char.* **2014,** *31*, 317-336.
32. Ko, M.; Chae S.; Cho J. Challenges in accommodating volume change of si anodes for li-ion batteries. *Chemelectrochem* **2015,** *2*, 1645-1651.
33. Liang, Y.; Tao, Z.; Chen, J. Organic Electrode Materials for Rechargeable Lithium Batteries.

Adv. Energy Mater. **2012,** 2, 742-769.

34. Xie, J.; Zhang, Q. Recent progress in rechargeable lithium batteries with organic materials as promising electrodes. *J. Mater. Chem. A.* **2016,** 4, 7091-7106.
35. Lin, D.; Liu, Y.; Yi, C. Reviving the lithium metal anode for high-energy batteries. *Nature Nanotechnology.* **2017,** 12, 194-206.
36. Luo, F.; Liu, B.; Zheng, J.; Chu, G.; Zhong, K.; Li, H.; Huang, X.; Chen, L; Review-Nano-Silicon/Carbon Composite Anode Materials Towards Practical Application for Next Generation Li-Ion Batteries. *J. Electrochem. Soc.* **2015,** 162, A2509-A2528.
37. Szczech, J. R.; Jin S. Nanostructured silicon for high capacity lithium battery anodes. *Energy Environ. Sci.* **2011,** *4*, 56-72.
38. Wu, H.; Cui, Y. Designing Nanostructured Si Anodes for High Energy Lithium Ion Batteries. *Nano Today* **2012**, 7, 414-429.
39. Zuo, X.; Zhu, J.; Peter, M. B.; Cheng, Y. J. Silicon based lithium-ion battery anodes: A chronicle perspective review. *Nano Energy,* **2017,** 31, 113-143.
40. Gonzalez, A. F.; Yang, N. H.; Liu, R. S. Silicon Anode Design for Lithium-ion Batteries: Progress and perspectives. *J. Phys. Chem. C.* **2017,** 121, 27775-27787.
41. Magasinski, A.; Dixon, P.; Hertzberg, B.; Kvit, A.; Ayala, J.; Yushin, G. High-performance lithium-ion anodes using a hierarchical bottom-up approach. *Nature Mater.* **2010,** 9, 353-358.

Chapter 2. Scalable method of selective extraction of high-quality nano-Si from industrial slag

2.1. Introduction

2.1.1. Nano-silicon

Silicon is one of the most attractive anode materials for Li-ion battery (LIB) system, because it exhibits high theoretical capacity (4200 mAh/g), which is 10 times higher than conventional graphite anode (372 mAh/g). However, silicon anode suffers from large volume change during charge and discharge process and low electrical conductivity. Thus, it is hard to use in practical LIBs.

To solve these problem, various researches have been done by structuring such as silicon nanotube, silicon film, and nano-silicon[2-3,5]. In case of nano-silicon, interestingly, under the 150 nm sized silicon particles do not show surface fracture and pulverization[4]. Moreover, nano-silicon enables deep lithiation into silicon core that is impossible in micro-silicon[6]. Even though nano-silicon has a lot of advantages, nano-silicon also had some problems such as too expensive synthesis cost and large surface area of nano-silicon.

Herein, we extracted high-quality nano-silicon from industrial slag by facile method. We used metallothermic reduction method for scalable synthesis of nano-silicon. And then, we used simple acid etching process to remove impurities. Finally, we extracted high-quality nano silicon. This nano-silicon effectively improve cycle performance in the Si anode.

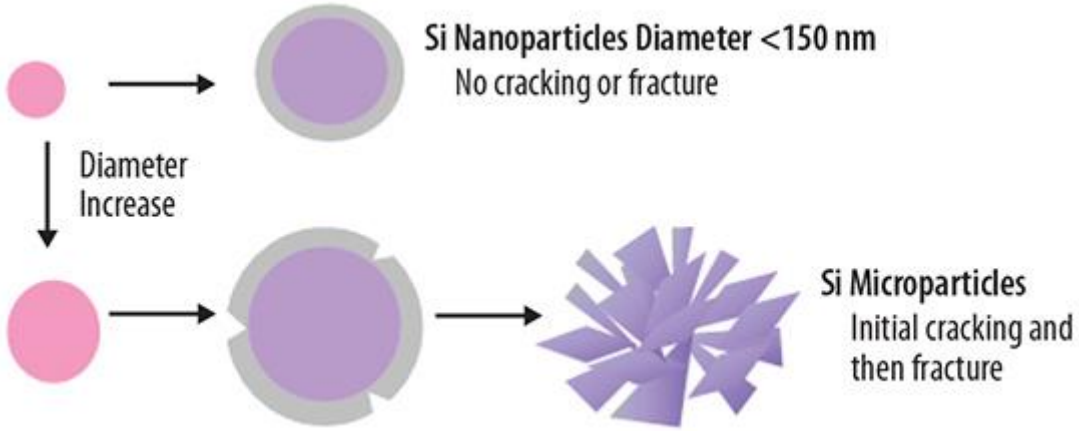

Figure 2.1. Schematic of the stability with silicon size during charge and discharge process[4].

2.1.2. Thermochemical reduction of SiO_2

Thermochemical reduction reaction is widely used in silicon synthesis[5,7-8]. In particular, metallothermic reduction reaction based on Ellingham diagram of metal oxide. Aluminum and magnesium can prefer oxidation rather than silicon. Therefore, SiO_2 can be reduced to silicon under aluminum or magnesium existence environment.

$$3SiO_2 + 4Al \rightarrow 3Si + 2Al_2O_3 \quad T \geq 900°C$$

$$SiO_2 + Mg \rightarrow Si + 2MgO \quad T \geq 600°C$$

However, these reactions required too high activation energy[8].

Here, if we use metal (e.g. aluminum, magnesiu, zinc) and metal halide (e.g. $AlCl_3$) complex, molten

$$3SiO_2 + 4Al \rightarrow 3Si + 2Al_2O_3 \quad \text{Path 0}$$

$$3SiO_2 + 6Al + 18AlCl_3 \rightarrow 3Si + 2Al_2O_3 + 6AlOCl \quad \text{Path a or b}$$

salt, then we can easily reduce the reaction activation energy[9].

Herein, we made high quality nano-silicon using a metallothermic reduction by using metal halide ($AlCl_3$). Participation of metal halide can reduce melting point of metal, leading facile molten salt system at low temperature. This system enables a low energetic reaction for reduction of silica. Also, this system confirmed by DFT simulation[9].

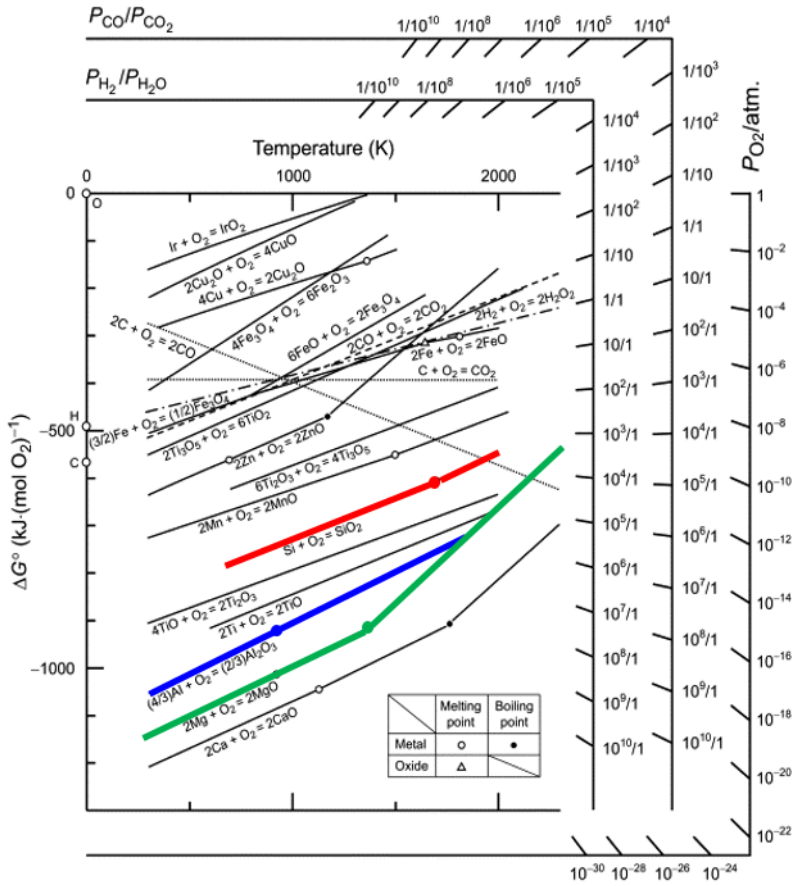

Figure 2.2. Ellingham diagram of metal oxide[10].

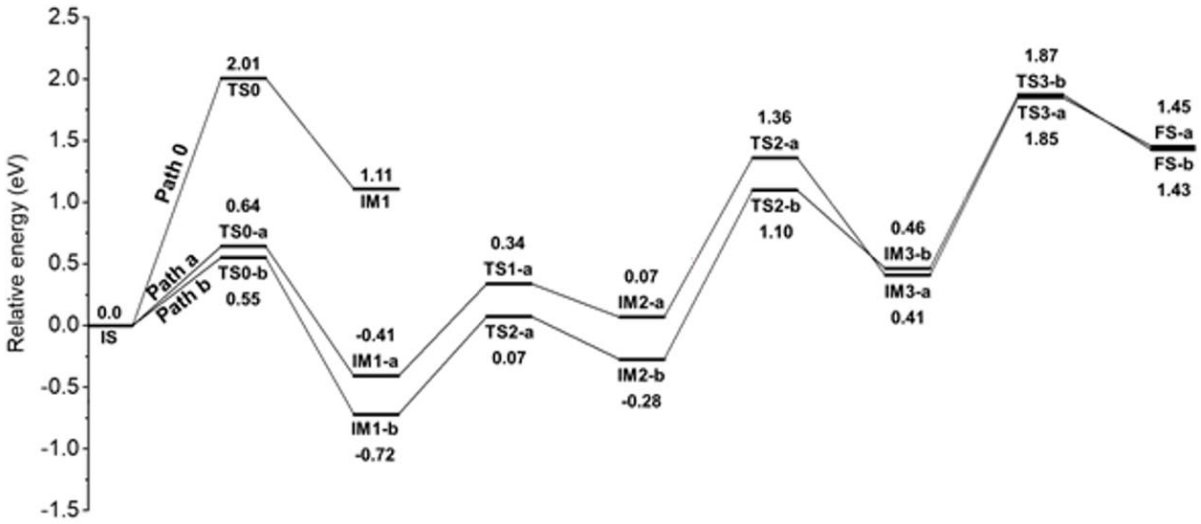

Figure 2.3. Reaction mechanism of silicon reduction[9].

2.2. Experimental Section

2.2.1. Extraction of Nano-silicon from industrial slag

First, dry slag powder at 70°C for 24h in oven to remove humidity. After dry the slag powder, dried slag powder (Posco Co., Ltd, South Korea), Al powder (3~5μm, Angang Steel Co., Ltd, China), and $AlCl_3$ powder(anhydrous, 95+%, Alfa Aesar) were mixed with a mass ratio 1:0.8:4 in Ar-filled glove box. After the mixing process, put the mixed powder into stainless steel reactor (UNILOK Co. Ltd, South Korea) in the Ar-filled glove box. Then the reactor was heated inside muffle furnace at 250°C for 16h. The obtained products were first washed in a H_2O/EtOH, and soaked in 3M HCl solution at 80°C for 5h to remove metal oxide. After HCl leaching, the product treated to 5 wt% HF solution to remove residual metal oxide and silica.

2.2.2. Material characterization

The morphology were obtained by scanning electron microscopy (SEM) (Verios 460, FEI). The local elemental analysis were obtained by EDS attached to the SEM apparatus. The X-ray diffraction (XRD) patterns were obtained by X-ray diffractometer (D8 ADVANCE, Bruker) using Cu-Kα radiation (λ = 1.5418 Å). A Raman spectrums were obtained by Raman spectrometer (alpha300R confocal microscope, WlTec) using a laser excitation wavelength of 532nm. The specific surface areas and pore sizes were obtained by automatic physisorption analyser (Micrometriticx, ASPS 2020).

2.2.3. Electrochemical test

The battery performance was measured by galvanostatic cycling (WonATech WBCS 3000 battery measurement system) of coin-type half cell (CR2016) with the extracted nano-silicon as the working electrode and lithium foil as the reference / counter electrode. The working electrodes were prepared using a conventional slurry method with a series of extracted nano-silicon, super P, 1:1 mixture of poly (acrylic acid) (PAA, weigh average molecular weight ~100K, Sigma-Aldrich), and sodium carboxymethyl cellulose (CMC, 6 wt% in H_2O, Sigma-Aldrich) as a binder with a mass ratio of 7:1.5:1.5. The mass loading of active materials, except conducting agent and binder, was ~ 0.91 mg cm^{-2} and ~ 2.73 mAh cm^{-2}. The potential windows for first cycled cells were between 0.005 and 1.5 V vs. Li/Li^+ and for the others cycled cells were 0.01 and 1.2 V vs. Li/Li^+. The electrolyte comprised 1.3M $LiPF_6$ in ethylene carbonate / diethyl carbonate, 3/7 volume ratio with 10wt% fluorinated ethylene carbonate additives. Polyethylene film (Celgard 2400) was used as a separator. Coin-type half cells (CR2016) were assembled in Ar-filled glove box.

2.3. Results and Discussion

Extraction procedure of nano-silicon is briefly described in Figure. 2.4. Previously, Lee et al. reported synthesis of porous silicon from industrial slag[11]. Figure 2.5 shows synthesis method of porous silicon from industrial slag[11]. However, our process is much more facile method than previously one. We just mixed slag powder, Al powder, and $AlCl_3$ powder and heated at 250 ºC for 16 h. After then, the product etched by HCl and HF solution to remove impurities. On the other hand, previous reported method has pre-treatment process ball-mill operation for 5 h and high concentration acid leaching at 80 ºC for 5 h to remove metal oxide[11]. After then, sample heated at 650 ºC for 2.5 h and etched by HCl and HF solution to remove impurities[11]. We simplified the synthesis method and extracted high-quality nano-silicon from industrial slag.

Figure 2.6 shows SEM images and EDS analysis in extraction process of slag. In EDS data of figure 2.6(a), slag has many impurities such as magnesium, aluminum, carbon, and calcium. These impurities perfectly removed after aluminothermic reduction and acid etching process. In figure 2.6. (d), extracted nano-silicon show 200~300 nm size, flake type morphology, 92.8 wt% of Si and 6.5 wt% of O.

Figure 2.7 shows XRD patterns and Raman spectrum of products. As the extraction progresses, impurities are perfectly removed and crystalline silicon appear. It can be checked in both XRD patterns and Raman spectrums. In figure 2.7(a), bare slag pattern shows amorphous metal oxide. However, HF-treated slag pattern shows crystalline silicon. In figure 2.7(b), as-reacted slag spectrum shows weak 520 nm^{-1} peak and strong 490 nm^{-1} peak. However, HF-treated slag spectrum shows strong 520nm^{-1} peak and weak 490 nm^{-1} peak. Here, in case of silicon, 520 nm^{-1} peak represent the crystalline silicon and 490 nm^{-1} peak represent the amorphous silicon. And also, because we extract nano-silicon, the Raman spectrums slightly shift to the right side.

Next, we have to check the specific surface area of extracted nano-silicon, we used Brunauer-Emmet-Teller (BET) and Barrett-Joyner-Halenda (BJH) analysis. Figure 2.8 shows BET and BJH analysis. According to the BET analysis, extracted nano-silicon particle have 39.2 m^2/g surface area and reference nano-silicon particle have 79.8 m^2/g surface area. Owing to lower surface area of extracted nano-silicon, it has lower possibility of side reaction between nano-silicon surface and electrolyte. Thus, it has higher initial columbic efficiency (ICE) than that of reference nano-silicon. In figure 2.9(a), extracted nano-silicon has 90.3%, ICE and reference nano-silicon has 80.2%, ICE. This is a natural result of the lower surface area that can reduce irreversible side reaction with the electrolyte of extracted nano-silicon. Figure 2.9(b) shows cycle performance of extracted nano-silicon. Reference nano-silicon had a capacity of 81.6 mAh/g and CE of 100% at the 20^{th} cycle and a capacity

of 15.8 mAh/g and CE of 100% at 100th cycle; this result indicates that capacity retention was 19.3%. Extracted nano-silicon had a capacity of 1292.8 mAh/g and CE of 99.8% at the 20th cycle and a capacity of 1151.0 mAh/g and CE of 99.0% at 100th cycle; this result indicates that capacity retention was 89.0%. Such an excellent cyclability of extracted nano-silicon originated from dispersibility and nanosize. First, our extracted nano-silicon particle have excellent dispersibility compare the reference nano-silicon paricle. Owing to its excellent dispersibility, our nano-silicon particle was uniformly well dispersed in the electrode. Second, 200~300nm sized small silicon prevent surface fracture and pulverization of silicon during charge and discharge process. Thus our nano-silicon shows higher ICE and excellent cyclability.

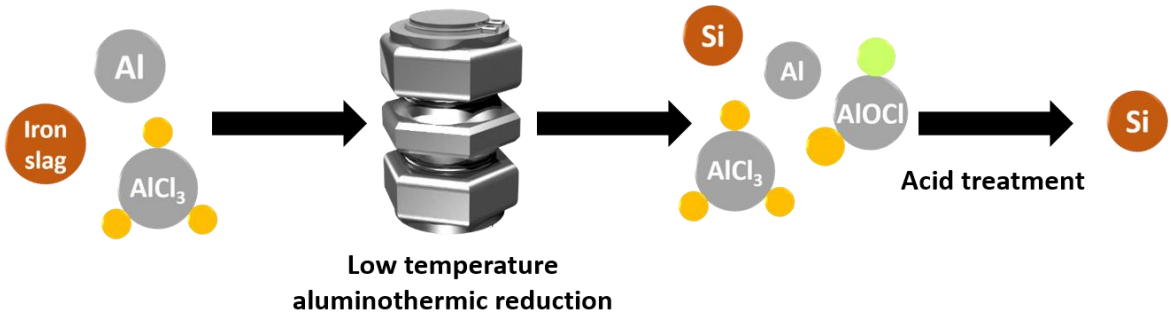

Figure 2.4. Schematic illustration of extraction of nano-silicon from industrial slag.

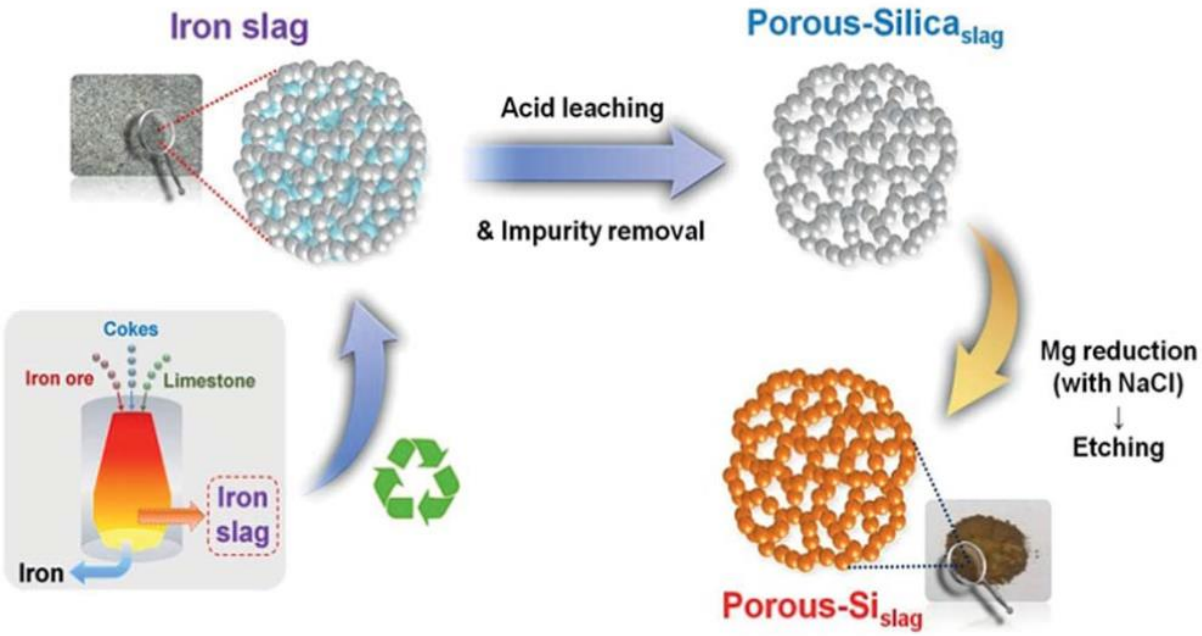

Figure 2.5. Schematic illustration of synthesis of porous silicon from industrial slag[11].

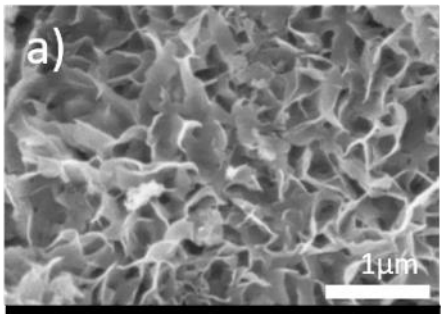

Element	Wt%	At%
Carbon	3.49	5.99
Oxygen	48.37	62.35
Magnesium	4.09	3.47
Aluminum	7.65	5.85
Silicon	15.73	11.53
Sulfur	1.19	0.76
Calcium	19.47	10.02

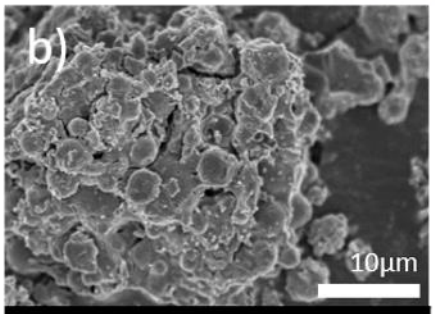

Element	Wt%	At%
Oxygen	32.91	45.12
Aluminum	58.86	48.24
Silicon	8.23	6.64

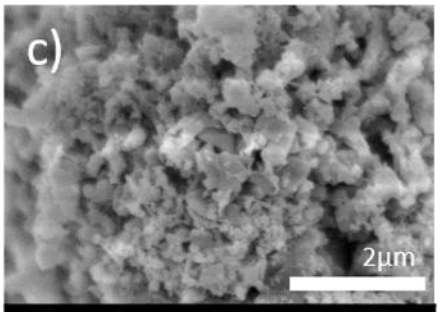

Element	Wt%	At%
Oxygen	30.60	45.36
Aluminum	5.06	4.36
Silicon	64.34	52.09

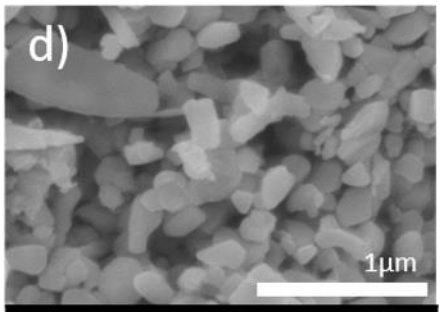

Element	Wt%	At%
Oxygen	6.50	10.88
Aluminum	0.73	0.73
Silicon	92.76	88.40

Figure 2.6. SEM images and EDS analysis of (a) slag, (b) as-reacted slag, (c) HCl-treated slag, and (d) HF-treated slag.

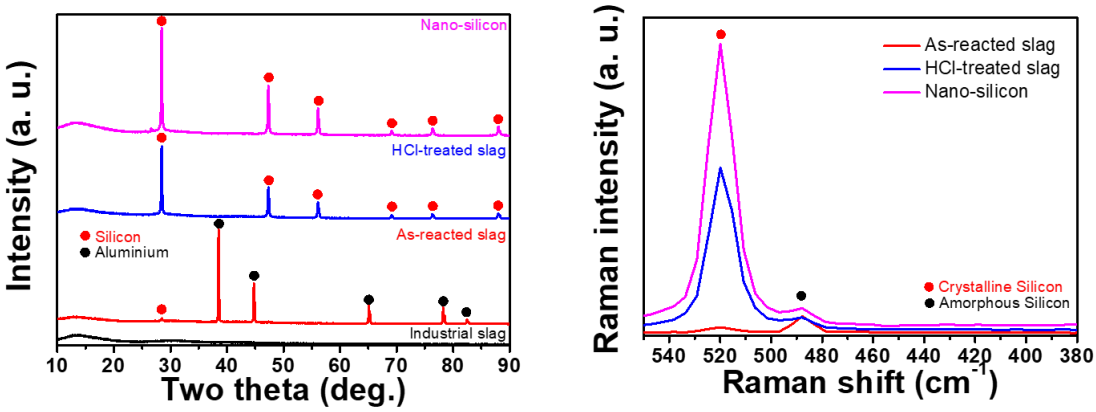

Figure 2.7. XRD patterns and Raman spectra of Nano-silicon.

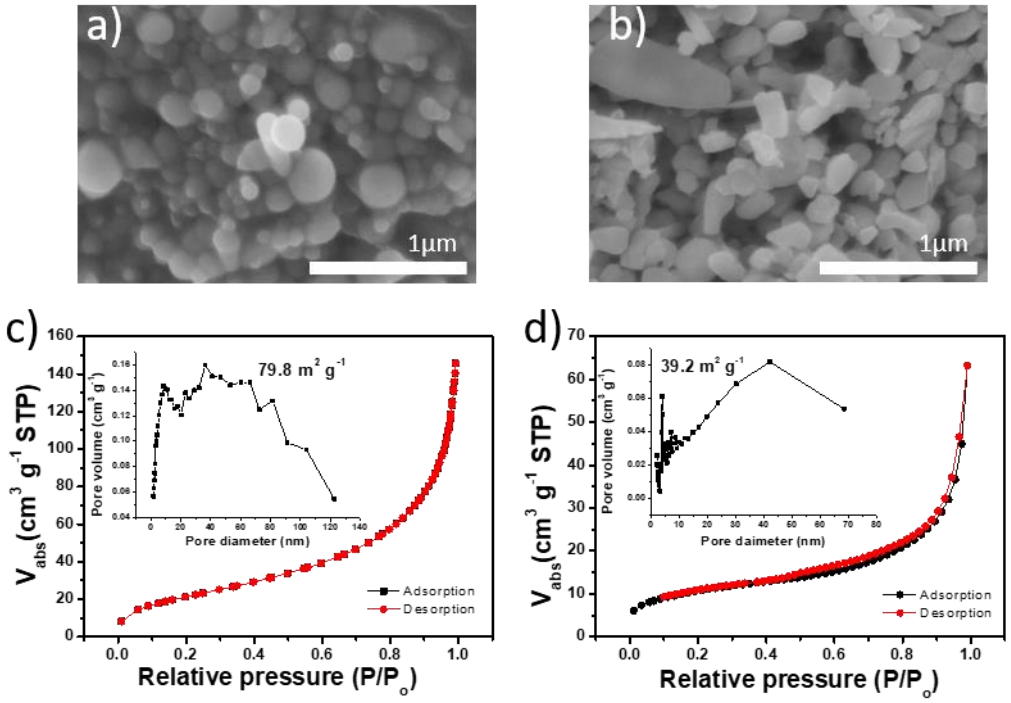

Figure 2.8. SEM image of (a) nano-silicon (ref), and (b) nano-silicon (syn). BET and BJH analysis of (a) nano-silicon (ref), and (d) nano-silicon (syn).

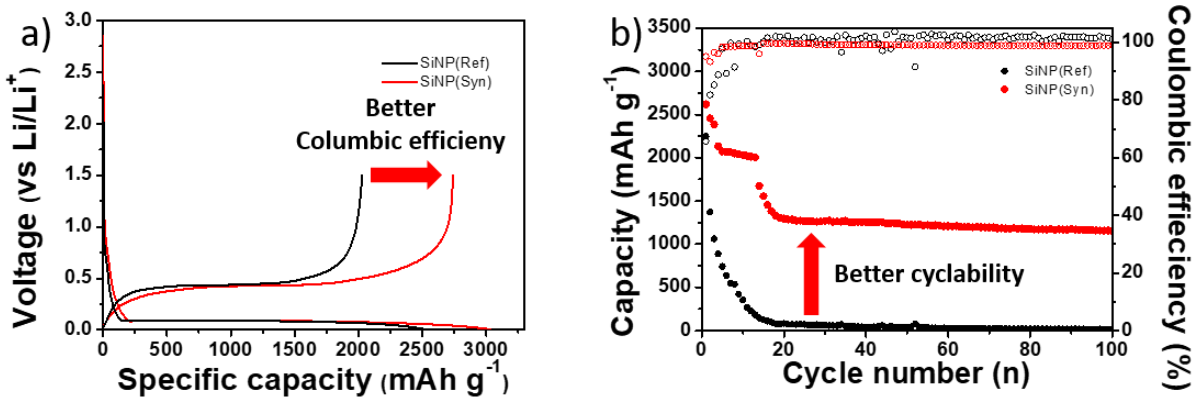

Figure 2.9. (a) Initial cycle of nano-silicon / Li cell (C-rate = 0.05C). (b) Cycle performance of nano-silicon / Li cell.

2.4. Conclusion

We demonstrate the cost-effective and facile synthesis method of nano-silicon from industrial slag. We easily synthesized high-quality nano-silicon. In addition, our synthesis method is very cost-effective way. This way can be effective way to synthesize nano silicon from various silicon sources. Based on the the theories, we reduce activation energy of metallothermic reduction for synthesis of nano-silicon. In the next chapter, I will introduce another strategy for enhanced performance in silicon anodes.

2.5. Reference

1. Zhao, K.; Pharr, M.; Wan, Q.; Wang. W. L.; Kaxiras, E.; Vlassak, J. J.; Suo, Z. Concurrent Reaction and Plasticity during Initial Lithiation of Crystalline Silicon in Lithium-Ion Batteries. *J. Electrochem. Soc.* **2012,** 159, A238-A243.
2. Chan, C. K.; Peng, H.; Liu, G.; Mcilwrath, K.; Zhang, X. F.; Huggins R. A.; Yi C. High-performance lithium battery anodes using silicon nanowires. *Nature Nanotech.* **2008,** 3, 31-35.
3. Yang, L.; Chen, H. S.; Jiang, H.; Wei, Y. J.; Song, W. L.; Fang, D. N. Failure mechnisms of 2D silicon film anodes: *in situ* observations and simulations on crack evolution. *Chem. Commun.* **2018,** 54, 3997-4000.
4. Liu, X. H.; Zhong, L.; Huang, S.; Mao, S. X.; Zhu, T.; Huang, J. Y. Size-Dependent Fracture of Siliocn Nanoparticles During Lithiation. *ACS Nano.* **2012,** 6, 1522-1531.
5. Cho W. C.; Kim H. J.; Lee H. I.; Seo M. W.; Ra H. W.; Yoon S. J.; Mun T. Y.; Kim J. H.; Kim B. H.; Kook J. W.; Yoo C.Y.; Lee J. G.; Choi J. W. 5L-Scale Magnesio_milling Reduction of Nanostructured SiO2 for High Capacity Silicon Anodes in Lithium-Ion Batteries. *Nano Lett.* **2016,** 16, 7261-7269.
6. Kalnaus, S.; Rhodes K.; Daniel C. A study of lithium ion intercalation induced fracture of silicon particles used as anode material in li-ion battery. *J. Power Sources* **2011,** *196*, 8116-8124.
7. Choi S. H.; Kim J.; Hwang D. Y.; Park H.; Ryu J.; Kwak S. K.; Park S. Generalized Redox-Responsive Assembly of Carbon-Sheathed Metallic and Semiconducting Nanowire Heterostructures. *Nano Lett.* **2016,** 16, 1179-1185.
8. Entwistle, J.; Rennie. A.; Patwardhan. S. A review of magnesiothermic reduction of silica to porous silicon for lithium-ion battery applications and beyond. *J. Mater. Chem. A.* **2018,** 6, 18344-18356.
9. Song G.; Ryu J.; Kim J. C.; Lee J. H.; Kim S.; Wang, C.; Kwak S. K.; Park S. Revealing salt-expedited reduction mechanism for hollow silicon microsphere formation in bi-functional halide melts. *Comm. Chem.* **2018,** 16, 7261.
10. Hasegawa, M.; Tratise on Process Metallurgy. *Elsevier.* **2014,** 1, 507-516.
11. Chun J.; An S.; Lee J. Highly mesoporous silicon derived from waste iron slag for high performance lithium ion battery anodes. *J. Mater. Chem. A.* **2015,** 3 21899-21906.

Chapter 3. Facile method of synthesis of unique structure Si/C composite

3.1. Introduction

3.1.1. Si-based composite

Silicon has the highest capacity of 4200 mAh/g that is more than 10 times higher than commercialized graphite anode (372 mAh/g)[1-2]. Owing to the highest capacity, Silicon is considered as one of the most promising anode materials for next-generation LIBs. However, owing to huge volume change during charge and discharge process and low electrical conductivity, it is hard to use in practical LIBs[3].

Nowadays, Si-based composite materials get much attention in LIBs[4-7]. Si-based composite materials consist of graphite, metal, and conductive materials supports and silicon[6-8]. Such Si-based composite material structure is physical mixture of support materials and silicon particles or silicon particles invaded in support materials frame[6-8]. Si-based composite materials synthesized by various method such as hydrothermal reaction, electrospray, and emulsion reaction[9-11].

Owing to structural characteristics of Si-based composite materials and support materials property, Si-based composite materials have some advantages in comparison with silicon such as structure stability, high tap density, and fast Li-ion and electron transfer[4-8].

Herein, we synthesized the unique structure Si/C composite material for LIB anode using polyacrylonitirle polymer and silicon chip. Using solvent-exchange method, we made porous structure in the Si/C composite inside. Also, oxidized silicon chip made York shell structure in the Si/C composite inside. Using these unique structures, we improved cycle performance of Si anode.

3.2. Experimental Section

3.2.1. Oxidation of silicon chip

10g of silicon chip powder were put into alumina boat. Then the alumina boat heated inside tube furnace at 500, 600, 700, 800, 950, and 1100ºC for 5h under air condition. After oxidation process, to make nano-silicon chip powder using ball-milling operation for 2h.

3.2.2. Synthesis of Si/C composite

0.5g of Polyacrylonitirile powder (PAN, weigh average molecular weight ~ 150K, Sigma-Aldrich) was dissolved in 4.5g of N,N-dimetylformamide solvent (DMF, anhydrous, 99.8%, Sigma-Aldrich). After making 10 wt% PAN solution, oxidized silicon chip powder, activated super P, and PAN solution were mixed with 0.4 g:20 mg:5 g with stirring at 130ºC. After mixing process, the solution were dropped into deionized water using syringe. The sample was filtered and rinsed with deionized water. The filtered sample was dried at 70 ºC for 24 h. After drying, the sample was put into alumina boat and heated in tube furnace at 250 ºC for 6 h under air condition and 900 ºC for 5 h under Ar condition. After carbonization process, the sample soaked in 10 wt% HF solution for 1 h to remove oxidation layer in silicon chip.

3.3.3. Material characterization

The morphology were obtained by scanning electron microscopy (SEM) (Verios 460, FEI). The local elemental analysis were obtained by EDS attached to the SEM apparatus. The X-ray diffraction (XRD) patterns were obtained by X-ray diffractometer (D8 ADVANCE, Bruker) using Cu-Kα radiation (λ = 1.5418 Å).

3.3.4. Electrochemical test

The battery performance was measured by galvanostatic cycling (WonATech WBCS 3000 battery measurement system) of coin-type half cells (CR2032) with the synthesized Si/C composite as the working electrode and lithium foil as the reference / counter electrode. The working electrodes were prepared using a conventional slurry method with a series of extracted nano-silicon, super P, 1:1 mixture of poly (acrylic acid) (PAA, weigh average molecular weight ~100K, Sigma-Aldrich), and sodium carboxymethyl cellulose (CMC, 6 wt% in H_2O, Sigma-Aldrich) as a binder with a mass ratio of 7:1.5:1.5. The mass loading of active materials, except conducting agent and binder, was ~ 1.13 mg cm^{-2} and ~ 1.02 mAh cm^{-2}. The potential windows for first cycled cells were between 0.005 and 1.5 V

vs. Li/Li^+ and for the others cycled cells were 0.01 and 1.2 V vs. Li/Li^+. The electrolyte comprised 1.3M $LiPF_6$ in ethylene carbonate / diethyl carbonate, 3/7 volume ratio with 10wt% fluorinated ethylene carbonate additives. Polyethylene film (Celgard 2400) was used as a separator. Coin-type half cells (CR2032) were assembled in Ar-filled glove box.

3.3. Results and Discussion

We used silicon chip, which is industrial waste of Si/SiC wafer as silicon source. In silicon, it is hard to be oxidized completely by thermal oxidation[12]. On the other hand, silicon carbide can easily oxidize completely by thermal oxidation[13]. Figure 3.1 shows scanning electron microscope (SEM) images of silicon chip and EDS analysis of silicon chip. According to the EDS analysis data, silicon chip has 13.16 At% of carbon. Using a silicon carbide property, which can be oxidized completely, we can control the amount of silicon chip's oxidation layer. Figure 3.2(a) shows change of silicon chip weight. As the thermal oxidation temperature increases, the amount of oxidation increases. Especially, at over 700 ºC, the amount of oxidation of silicon chip increase rapidly. According to these data, we can easily control the amount of oxidation of silicon chip. Figure 3.2(b) shows XRD patterns of oxidized silicon chips. As the oxidation progresses, XRD peak shift to the right. This is very natural phenomena. Because, as the oxidation progresses, silicon chip make SiO_x, then d-spacing should be d-space should be shorter. Thus, XRD peak shift to the right. Finally, at 1100 ºC, silicon chip make SiO_2.

Synthesis procedure of Si/C composite is briefly described in Figure 3.3. First, we prepared polyacrylonitrile (PAN) solution in DMF. Then put oxidized silicon chip and activated super P into PAN solution. Here, we use activation super P to increase conductivity in Si/C composite and use HNO_3 to activate super P. And activated super P shows improved dispersibility. Then drop the PAN solution into deionized water. This process described in figure 3.4. PAN solution was solidified when it contacts with deionized water. At the same time, DMF solvent escape from solidified sample, then make small pore in the sample[14]. These small pores accommodated the volume expansion of silicon during charge and discharge process. After then, we got 4~5mm sized silicon chip@PAN sample. This sample heated in the tube furnace at 900ºC for 3h to carbonize PAN. After carbonization process, 1~2mm sized sample soaked into 10 wt% of HF solution to remove oxidation layer at silicon chip. Then we got unique structured Si/C composite. Figure 3.5 shows SEM images of samples. In figure 3.5(c) and (d), we can check unique structured Si/C composite, inner nano pores. This Si/C composite was easily grinded by hand. Grinded Si/C composite shows 1~3 μm regular size. And we made SiC free Si/C composite. In figure 3.7, Si/C composite shows crystalline silicon peaks and amorphous graphite peaks. However, there is no SiC peaks. If Si/C composite make SiC, then (1 1 1) plane peak of SiC would be appeared at the two theta is 36º.

Finally, figure 3.8 shows electrochemical test result of Si/C composite cell. In figure 3.8(a), bare silicon chip shows 87.9% initial columbic efficiency (ICE). Si/C composite shows 81.5% ICE, it is 6.4% lower than that of silicon chip. Owing to large amount of vacancy site in the Si/C composite, ICE value decreased in the Si/C composite. In figure 3.8(b), bare silicon chip had a capacity of 2010.3 mAh/g and CE of 99.1% at the 10^{th} cycle and a capacity of 950.2 mAh/g and CE of 100.5% at the 100^{th} cycle; this result indicates that capacity retention was 47.3%. Si/C composite had a capacity of 1446.1 mAh/g and CE of 98.6% and a capacity of 1149.1 mAh/g and CE of 99.4% at the 100^{th} cycle; this result indicates that capacity retention was 79.5%. Such an excellent cyclability of Si/C composite originated from unique structure of Si/C composite. Our Si/C composite composed of two type of vacancy. First one is Yolk shell vacancy come from oxidation layer of silicon chip. The other one is nano-pore inside the Si/C composite come from solvent-exchange. Thus our unique structured Si/C composite shows excellent cyclability.

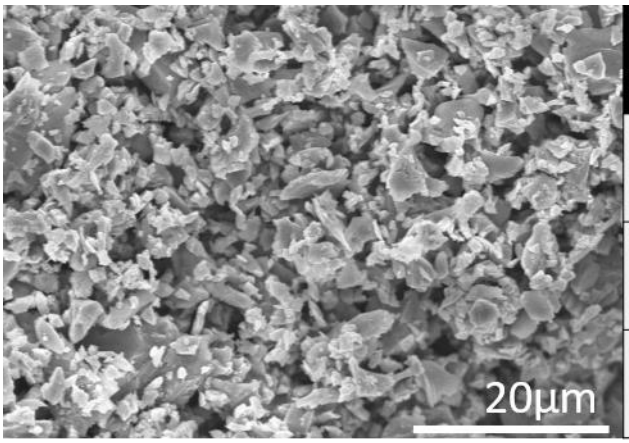

Element	Wt(%)	At(%)
Carbon	6.17	13.16
Oxygen	1.92	3.08
Silicon	91.90	83.76

Figure 3.1. Characterization of silicon chip. SEM image and EDS analysis.

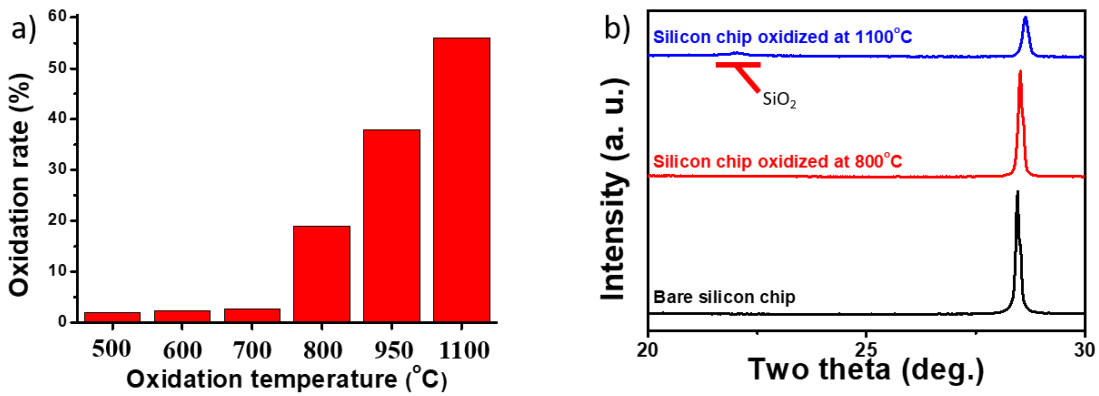

Figure 3.2. Change of silicon chip (a) weight, and (b) XRD patterns at various temperature.

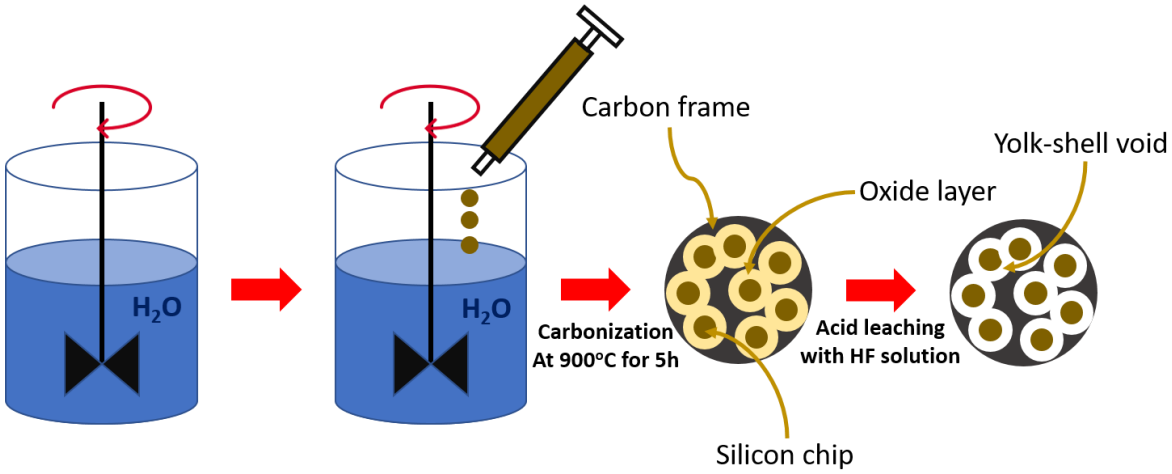

Figure 3.3. Schematic illustration of synthesis of Si/C composite.

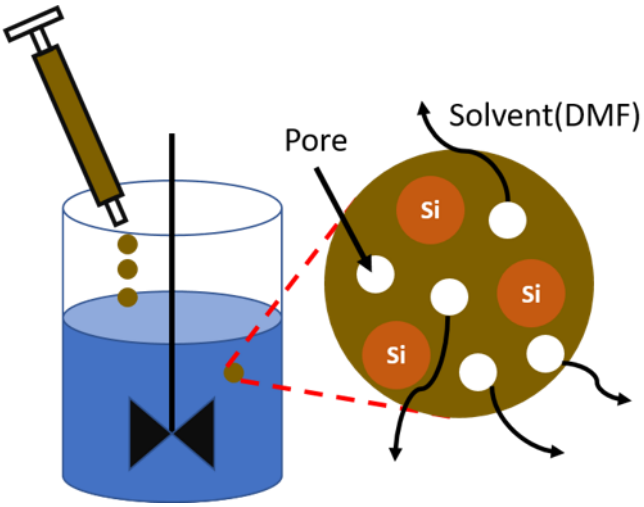

Figure 3.4. Schematic illustration of principle of nano-pore generation in Si/C composite.

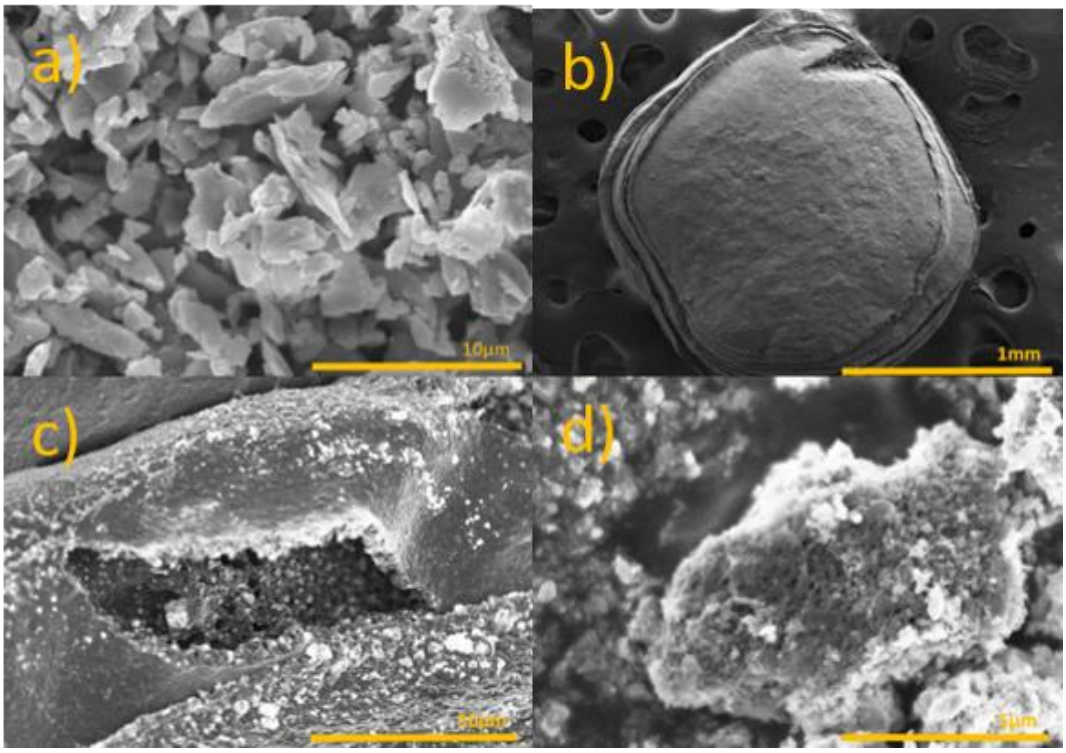

Figure 3.5. SEM images of (a) silicon chip, (b) silicon chip@PAN, and (c),(d) Si/C composite.

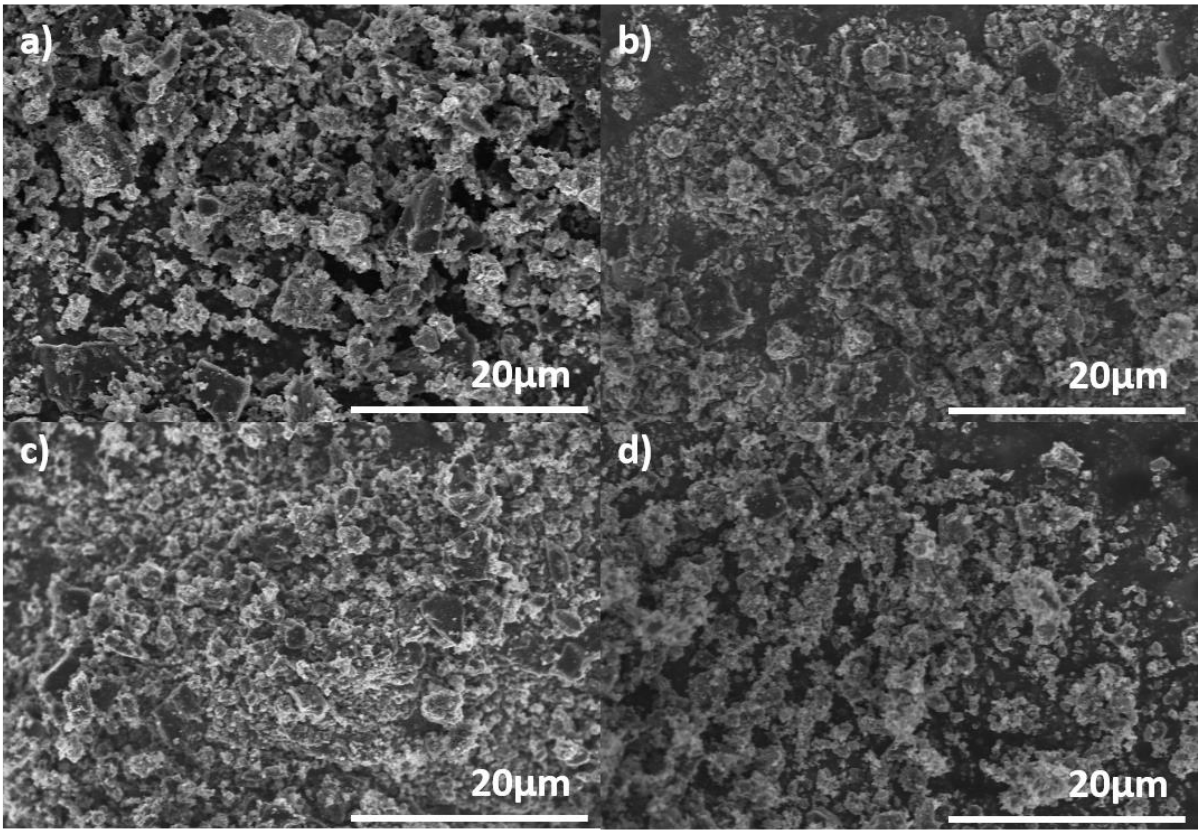

Figure 3.6. SEM images of Si/C composites grinded by hand. (a) 3 min, (b) 6 min, (c) 9 min, and (d) 12 min.

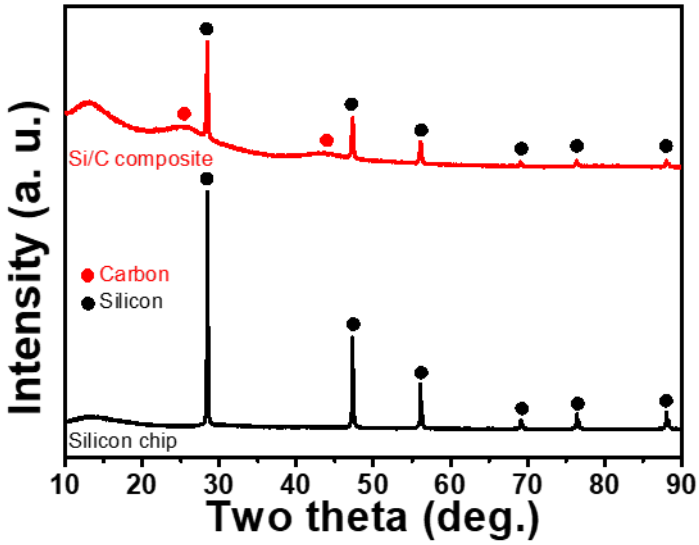

Figure 3.7. XRD patterns of (a) silicon chip and (b) Si/C composite.

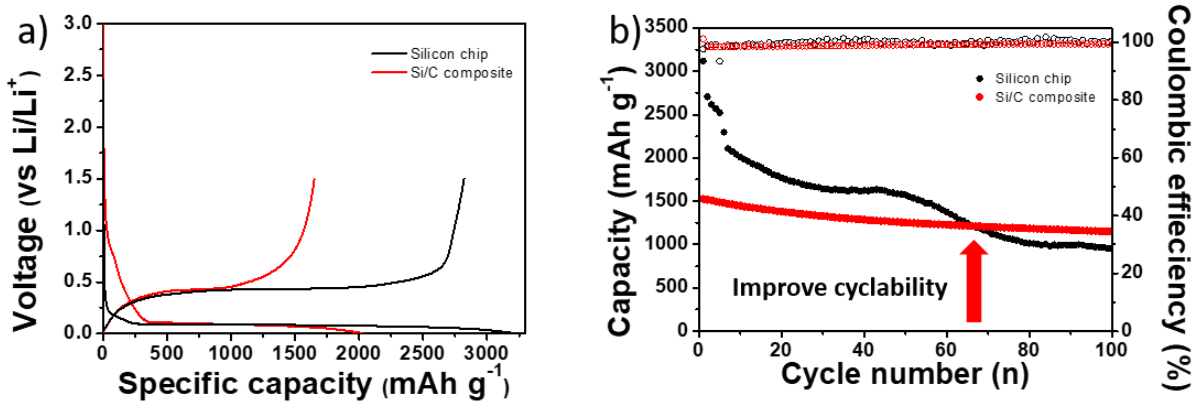

Figure 3.8. (a) Initial cycle of Si/C composite / Li cell (C-rate = 0.05C). (b) Cycle performance of Si/C composite / Li cell.

3.4. Conclusion

We demonstrated Si/C composite for Li-ion battery system (LIBs) anode. First, using oxidized silicon chip as silicon, we can easily make York shell structure in the Si/C composite. Second, using solvent-exchange method, we can easily, make large amount of pore in the Si/C composite. These vacancies effectively accommodate the volume expansion of silicon during charge and discharge process. Carbonized polyacrylonitrile (PAN) and small amount of super P effectively increased conductivity of Si/C composite. Finally, unique structured Si/C composite synthesized by facile method effectively increased cycle performance.

3.5. Reference

1. McDowell, M. T.; Lee S. W.; Nix W. D.; Cui Y. 25th anniversary article: Understanding the lithiation of silicon and other alloying anodes for lithium-ion batteries. *Adv. Mater.* **2013,** *25*, 4966-4984.
2. Szczech, J. R.; Jin S. Nanostructured silicon for high capacity lithium battery anodes. *Energy Environ. Sci.* **2011,** *4*, 56-72.
3. Ko, M.; Chae S.; Cho J. Challenges in accommodating volume change of si anodes for li-ion batteries. *Chemelectrochem* **2015,** *2*, 1645-1651.
4. Lee J. K.; Oh C.; Kim N.; Hwang J. Y.; Sun Y. K. Rational design of silicon-based composites for high-energy storage devices. *J. Mater. Chem. A.* **2016,** 4, 5366-5384.
5. Luo, F.; Liu, B.; Zheng, J.; Chu, G.; Zhong, K.; Li, H.; Huang, X.; Chen, L; Review-Nano-Silicon/Carbon Composite Anode Materials Towards Practical Application for Next Generation Li-Ion Batteries. *J. Electrochem. Soc.* **2015,** 162, A2509-A2528.
6. Terranova, M. L.; Orlanducci, S.; Tamburri, E.; Guglielmotti, V.; Rossi, M. Si/C hybrid nanostructures for Li-ion anodes: An overview. *J. Power Source.* **2014,** 246, 167-177.
7. Yang, J.; Wang, B. F.; Wang, K.; Liu, Y.; Xie, J. Y.; Wen, Z. S. Si/C Composites for high Capacity Lithium Storage Materials. *J. Electrochem. Soc.* **2003,** 6, A154-A156.
8. Chae S.; Kim N.; Ma J.; Cho J.; Ko M. One-to-One Comparison of Graphite-Blended Negtive Electrodes Using Silicon Nanolayer-Embedded Graphite versus Commercial Benchmarking Materials for High-Energy Lithium-Ion Batteries. *Adv. Energy Mater.* **2017,** 7, 1700071.
9. Jeong M. G.; Du, H. L.; Islam, M.; Lee J. K.; Sun Y. K.; Jung H. G. Self-Rearrangement of Silicon Nanoparticles Embedded in Micro-Carbon Sphere Framework for High-Energy and Long-Life Lithium-Ion Batteries. *Nano Lett.* **2017,** 17, 5600-5606.
10. Xu, Q.; Sun J. K.; Yin Y. X.; Guo Y. G. Facile Synthesis of Blocky SiO_x/C with Graphite-Like Structure for High-Performance Lithium-Ion Battery Anodes. *Adv. Funct. Mater.* **2018,** 28, 1705235.
11. Lee S. J.; Kim H. J.; Hwang T. H.; Choi S.; Park S. H.; Deniz, E.; Jung D. S.; Choi J. W. Delicate Structural Control of Si-SiO_x-C Composite via High Speed Spray Pyrolysis for Li-Ion Battery Anodes. *Nano Lett.* **2017,** 17, 1870-1876.
12. Karube, N.; Yamamoto, K.; Kamiyama, M.; Thermal oxidation of silicon. *Jpn. J. Appl. Phys.* **1963,** 2, 11-18.
13. Roy, J.; Chandra, S.; Das, S.; Maitra, S. OXIDATION BEHAVIOUR OF SILICON CARBIDE – A REVIEW. *Rev. Adv. Mater. Sci.* **2014,** 38, 29-39.

14. Holda, A. K.; Ivo F. J.; Vankelecom, F. J. Understanding and guiding the phase inversion process for synthesis of solvent resistant nanofiltration membranes. *J. Appl. Polym. Sci.* **2015,** 132, 42130.